Surface-directed phase separation with off-critical composition: Analytical and numerical results

Sanjay Puri[1] and Kurt Binder[2]
[1]*School of Physical Sciences, Jawaharlal Nehru University, New Delhi 110067, India*
[2]*Institut für Physik, Johannes-Gutenberg-Universität Mainz, Staudinger Weg 7, 55099 Mainz, Germany*
(Received 24 July 2002; published 10 December 2002)

We study the interplay of wetting and phase separation in an unstable binary mixture (AB) with off-critical composition, placed in contact with a surface which prefers the component A. We consider surface potentials $V(z) \sim z^{-n}$, where z is the distance from the surface, and present analytical arguments and detailed numerical results to elucidate wetting-layer kinetics for arbitrary mixture compositions. If the preferred component is the minority phase, the wetting-layer thickness exhibits a potential-specific behavior at early times τ, $R_1 \sim \tau^{1/(n+2)}$, before crossing over to the universal growth law, $R_1 \sim \tau^{1/3}$. On the other hand, if the preferred component is the majority phase, there is a crossover from potential-specific growth (as before) to a slower growth regime.

DOI: 10.1103/PhysRevE.66.061602 PACS number(s): 68.05.−n

I. INTRODUCTION

Consider a binary mixture (AB), which is homogeneous at high temperatures and phase-separated at low temperatures. If the mixture is rapidly quenched from the one-phase region of the phase diagram to the two-phase region, it evolves towards the phase-separated state via a nonlinear phase ordering process [1–3]. Much research interest has focused on this far-from-equilibrium evolution, and there now exists a good understanding of phase ordering dynamics for bulk binary mixtures. Typically, the segregating system coarsens into A-rich and B-rich domains, which are characterized by a growing length scale $L(\tau) \sim \tau^{\phi}$, where τ is the time after the quench. The growth exponent $\phi = 1/3$ when coarsening is driven by a diffusive mechanism, as in solid mixtures. This growth law is referred to as the Lifshitz-Slyozov or LS law [4]. For fluid mixtures, the hydrodynamic velocity field provides additional modes of material transport. Droplet diffusion and coagulation also yields a growth exponent $\phi = 1/3$, and constitutes the dominant growth mechanism when the coarsening morphology is not bicontinuous [5]. However, if the phase-separating fluid has an interconnected morphology, there are various growth regimes with crossovers from $\phi = 1/3$ (diffusive) $\rightarrow \phi = 1$ (viscous hydrodynamic) $\rightarrow \phi = 2/3$ (inertial hydrodynamic) [6,7].

Apart from the domain growth laws, experimentalists are also interested in quantitative features of the phase-separating morphologies—as reflected in the time-dependent structure factor $S(\vec{k}, \tau)$ ($\vec{k}$ being the wave vector) or its Fourier transform, the correlation function. In the limit where one of the components is present in a vanishingly small fraction, these quantities were analytically obtained by Lifshitz and Slyozov [4]. However, our understanding of the structure factor is relatively limited in the case where appreciable fractions of both components are present. We understand the behavior of $S(\vec{k}, \tau)$ in the limits $k \rightarrow 0$ and $k \rightarrow \infty$ [2,3], but there is no comprehensive theory for intermediate values of k [8].

Next, let us focus on the experimentally important problem of an immiscible binary mixture (AB) in contact with a surface (S) with a preferential attraction for one of the components of the mixture (say, A). Let γ_A, γ_B, and σ denote the surface tensions between A-S, B-S, and A-B, respectively. Then, the contact angle θ between A and S is obtained as the solution of $\sigma \cos\theta = \gamma_B - \gamma_A$ [9]. This equation has no solution if $\gamma_B - \gamma_A > \sigma$, which corresponds to a situation where the component A completely wets the surface [completely wet (CW) morphology]. For $\gamma_B - \gamma_A < \sigma$, both A and B are in contact with the surface in a partially wet (PW) morphology, though there is a surplus of the preferred component A at the surface. The equilibrium transitions between PW and CW morphologies, and the effects of geometry and composition, have been extensively studied in the literature [10–12].

In this paper, we will focus on the following dynamical problem. Consider a homogeneous mixture AB (at high temperature) in contact with a surface which prefers A. At time $\tau = 0$, the system is quenched deep below the miscibility gap. The subsequent evolution of the system is characterized by (a) bulk phase separation; (b) kinetics of wetting at the surface; and (c) the dynamical interplay of surface wetting and bulk phase separation.

This problem is of great experimental interest, and was first studied by Jones *et al.* [13] in the context of phase-separating polymer mixtures in a ''semi-infinite'' geometry. These authors examined laterally averaged composition profiles as a function of distance from the wetting surface. In the bulk, the lateral-averaging procedure does not yield a systematic behavior because the phase-separation profiles have randomly oriented wave vectors. However, at the surface, there is a wetting layer of the preferred component, which is followed by a depletion layer, etc. The surface morphology is time dependent and propagates into the bulk. There have been many subsequent experiments on this problem [14,15], and some of these are reviewed by Krausch [16].

The first phenomenological model of surface-directed phase separation was proposed by Puri and Binder [17], and will be discussed in Sec. II. It consists of (a) the Cahn-Hilliard-Cook (CHC) model for bulk phase separation supplemented with a surface-potential term; and (b) two boundary conditions on the order parameter at the surface. This and similar models have been studied analytically and

numerically by various authors [18–23], and some of these works have been reviewed by Puri and Frisch [24] and Binder [25]. Most of these studies have focused on mixtures with critical composition, and there have been few studies of the off-critical case [23,19].

The experimental and numerical studies of this problem have reported a wide range of growth exponents for the wetting-layer dynamics. In a recent paper [26], we have attempted to systematize these observations in the context of segregation driven by diffusive processes. In particular, we have focused on the crossovers from potential-specific growth to universal growth; and the role of mixture composition in determining growth laws and crossovers. This paper is an expanded version of Ref. [26]. It presents many important results for a broad range of compositions, and contains a pedagogical exposition of the issues discussed in our earlier paper.

This paper is organized as follows. Section II discusses our modeling of surface-directed phase separation, and presents numerical details regarding our simulations. In Sec. III, we present detailed analytical and numerical results. Section IV concludes this paper with a summary and discussion of our results.

II. MODELING OF SURFACE-DIRECTED PHASE SEPARATION

Consider a binary mixture (AB) in contact with a surface located at $z=0$. This physical system is described by the semi-infinite Ising model. To mimic the phase separation of a binary mixture, we associate stochastic spin-exchange kinetics with the Ising model by placing it in contact with a heat bath. The master equation for this stochastic evolution can be used to obtain an evolution equation for the coarse-grained order parameter [27,28]. Details of this procedure in the present context are provided in earlier publications [17,28] and we do not replicate them here. The resultant model is the usual CHC model for bulk phase separation, which has the following form (in dimensionless units):

$$\begin{aligned}\frac{\partial\phi(\vec{x},\tau)}{\partial\tau} &= -\vec{\nabla}\cdot\vec{J}(\vec{x},\tau)\\ &= -\vec{\nabla}\cdot\{-\vec{\nabla}\mu(\vec{x},\tau)+\vec{\xi}(\vec{x},\tau)\}\\ &= -\vec{\nabla}\cdot\left\{\vec{\nabla}\left[\phi(\vec{x},\tau)-\phi(\vec{x},\tau)^3+\frac{1}{2}\nabla^2\phi(\vec{x},\tau)\right.\right.\\ &\quad\left.\left.+V(z)\right]+\vec{\xi}(\vec{x},\tau)\right\},\end{aligned} \tag{1}$$

where $\phi(\vec{x},\tau)\equiv\phi(\vec{\rho},z,\tau)$ is the order parameter, which depends on dimensionless space $\vec{x}$ and time τ. The spatial variable is decomposed into $(d-1)$ variables $\vec{\rho}$ parallel to the wall (d being dimensionality), and one variable z (>0) perpendicular to the wall. In Eq. (1), the order parameter locally saturates to its equilibrium values of $\phi^*=+1$ (corresponding to A, say) and $\phi^*=-1$ (corresponding to B). However, the evolution conserves the overall composition, i.e., $V^{-1}\int d\vec{x}\,\phi(\vec{x},\tau)=\phi_0$, where V is the system volume and ϕ_0 is the average order parameter. The quantities $\vec{J}(\vec{x},\tau)$ and $\mu(\vec{x},\tau)$ in Eq. (1) refer to the current and chemical-potential difference between A and B, respectively.

In Eq. (1), $V(z)$ denotes the surface potential. We have studied both short-ranged (delta function or exponential) and power-law potentials. Here, we present results for the power-law case,

$$\begin{aligned}V(z) &= h_1, \quad z\leqslant 1,\\ &= \frac{h_1}{z^n}, \quad z>1,\end{aligned} \tag{2}$$

where we introduce a lower cutoff to avoid the power-law singularity at $z=0$. This cutoff is placed at $z=1$, rather than at some ''small'' value, as our numerical discretization of Eq. (1) (described below) will use a large mesh size $\Delta x=1$ in all coordinate directions. Such potentials are ubiquitous in the context of surface-molecule interactions, e.g., $n=\kappa-d$, with $\kappa=6$ and 7 corresponding to cases with nonretarded and retarded van der Waals' interactions, respectively [29,30]. Clearly, the short-ranged case is recovered in the limit $n\to\infty$.

The thermal fluctuations in Eq. (1) are modeled by Gaussian white noise with zero mean,

$$\begin{aligned}\langle\xi_i(\vec{x},\tau)\rangle &= 0, \quad i=1\to d,\\ \langle\xi_i(\vec{x},\tau)\xi_j(\vec{x}',\tau')\rangle &= \epsilon\delta_{ij}\delta(\vec{x}-\vec{x}')\,\delta(\tau-\tau'),\end{aligned} \tag{3}$$

where ϵ measures the noise strength. The quantity ϵ is related to system parameters as [17,24]

$$\epsilon=\frac{2}{3}\left(\frac{T_c}{T}-1\right)^{-2}\xi_b^{-d}, \tag{4}$$

where T_c is the bulk critical temperature, T is the quench temperature, and ξ_b is the bulk correlation length. In mean-field theory, $\xi_b=\sqrt{2/q}(1-T/T_c)^{-1/2}$, where q is the coordination number of the lattice.

Finally, we must supplement Eq. (1) with boundary conditions at $z=0$, as follows [17,18]:

$$\frac{\partial\phi(\vec{\rho},z=0,\tau)}{\partial\tau}=V(0)+g\,\phi(\vec{\rho},z=0,\tau)+\gamma\left.\frac{\partial\phi}{\partial z}\right|_{z=0}, \tag{5}$$

$$0=\left\{\frac{\partial}{\partial z}\left[\phi-\phi^3+\frac{1}{2}\nabla^2\phi+V(z)\right]+(\text{noise})\right\}_{z=0}. \tag{6}$$

Equation (5) rapidly relaxes the surface value of the order parameter to its equilibrium value—we will use its static version here. Equation (6) corresponds to zero current across the plane $z=0$, and enforces conservation of the order parameter. In general, the parameters h_1,n,ϵ,g,γ determine the equilibrium phase diagram of the surface [24,31]. Note that both first- and second-order wetting transitions are described by our model—we will always operate in the most interesting regime, above the temperature of the wetting transition, where the surface is completely wetted by the preferred component.

The model described above is appropriate for a semi-infinite geometry. The extension to a thin-film (or other) geometry is straightforward—the boundary conditions in Eqs. (5) and (6) have to be implemented on all surfaces. The thin-film geometry gives rise to many important physical features because of the interaction of surface-directed waves arising from different boundaries [32].

Next, it is relevant to discuss details of our Langevin simulation techniques. We implemented an Euler-discretized version of Eq. (1) with isotropic Laplacians and derivatives on a $d=2$ square lattice of size $N_x \times N_z$. The discretization mesh sizes in space and time were $\Delta x=1$ and $\Delta \tau=0.03$, respectively. The rather large mesh size in space is reasonable as it is smaller than the intrinsic thickness of the interface between regions of coexisting phases. Furthermore, all other length scales in our simulations (e.g., domain size and wetting-layer thickness) diverge with time.

The boundary conditions in Eqs. (5) and (6) were imposed at $z=0$, and flat boundary conditions were imposed at $z=N_z$, viz.,

$$\phi(x,N_z+1,\tau)=\phi(x,N_z-1,\tau),$$

$$J_z(x,N_z,\tau)=J_z(x,N_z+1,\tau)=0, \tag{7}$$

where the z component of the current is identified from Eq. (1). Periodic boundary conditions are imposed in the x direction.

The parameter values in our simulations were chosen as follows. We consider a nonretarded van der Waals' potential with $n=4$ (in $d=2$) and $h_1=0.8$. The other parameter values were $g=-0.4$ and $\gamma=0.4$, corresponding to complete wetting in equilibrium [24,31]. Finally, thermal noise of strength ϵ is mimicked by uniformly distributed random numbers between $[-A_n, A_n]$. The appropriate noise amplitude in our Langevin simulation is

$$A_n=\sqrt{\frac{3\epsilon}{(\Delta x)^d \Delta \tau}}. \tag{8}$$

Our $d=2$ simulations are performed for either $\epsilon=0$ ($T=0$); or $\epsilon=0.0817$ ($A=2.858$ for $\Delta x=1$ and $\Delta \tau=0.03$), which corresponds to a deep quench with $T \simeq 0.22 T_c$ from Eq. (4). We have also done simulations with Gaussian-distributed noise, and the results are equivalent to those presented here.

In the following section, we will show evolution pictures resulting from homogeneous initial conditions, with $\phi(\vec{x},0)$ consisting of small-amplitude uniformly distributed fluctuations about a background value (or off criticality) ϕ_0. We will also present laterally averaged order-parameter profiles and study their quantitative characteristics. All statistical data presented in this paper are obtained as an average over 200 independent runs.

III. ANALYTICAL AND NUMERICAL RESULTS

Let us now present detailed analytical and numerical results. All numerical results are presented for the noisy case, unless stated otherwise. As discussed earlier, we are primarily interested in off-critical quenches ($\phi_0 \neq 0$), where there is an asymmetry in the composition. The case of a critical quench ($\phi_0=0$) has already been studied extensively [17,18,20,21].

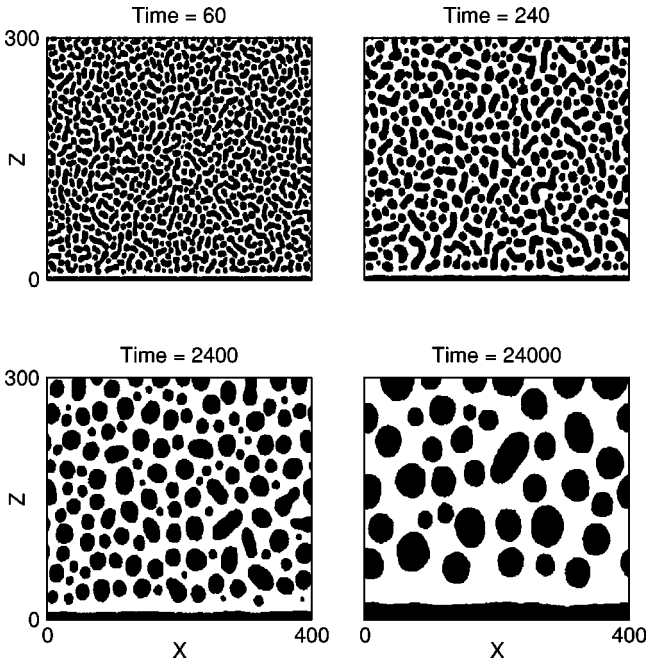

FIG. 1. Evolution of a homogeneous binary mixture (AB) from our model in Eqs. (1), (5), and (6). The simulation details and parameters are discussed in the text. The system size was $N_x \times N_z$ ($N_x=400$, $N_z=300$), and the surface which prefers A ($\phi>0$, marked in black) is located at $z=0$. The initial condition for $\phi(\vec{x},0)$ consisted of small-amplitude random fluctuations about a background value $\phi_0=-0.2$. For our choice of parameters, the surface is completely wetted by A. We show evolution pictures at four different times, as indicated.

A. Minority component wets the surface ($\phi_0<0$)

1. Evolution pictures and laterally averaged profiles

Figure 1 shows the evolution from a homogeneous initial condition for $\phi_0=-0.2$, corresponding to a mixture with 40% A (the preferred component) and 60% B. The system size is $N_x=400$, $N_z=300$. The surface is located at $z=0$, and we show evolution snapshots at four different times. Let us focus on the final frame at $\tau=24\,000$. The bulk (large z) is characterized by the usual droplet morphology for off-critical phase separation [33]. There is a wetting layer of the preferred component at the surface, which is followed by a depletion layer. Figure 2(a) shows laterally averaged profiles as a function of depth from the surface, $\phi_{\rm av}(z,\tau)$ vs z, corresponding to the snapshots in Fig. 1. [Figure 2(a) is comparable to the averaged profiles in the experiments of Jones *et al.*, cf. Fig. 1 of Ref. [13].] The averaging procedure gives $\phi_{\rm av}(z,\tau) \simeq \phi_0$ in the bulk, where the phase-separation profiles are randomly oriented. At the surface, there is a systematic wetting profile, as discussed earlier. We will characterize this profile by the zero crossings of $[\phi_{\rm av}(z,\tau)-\phi_0]$—$R_1(\tau)$

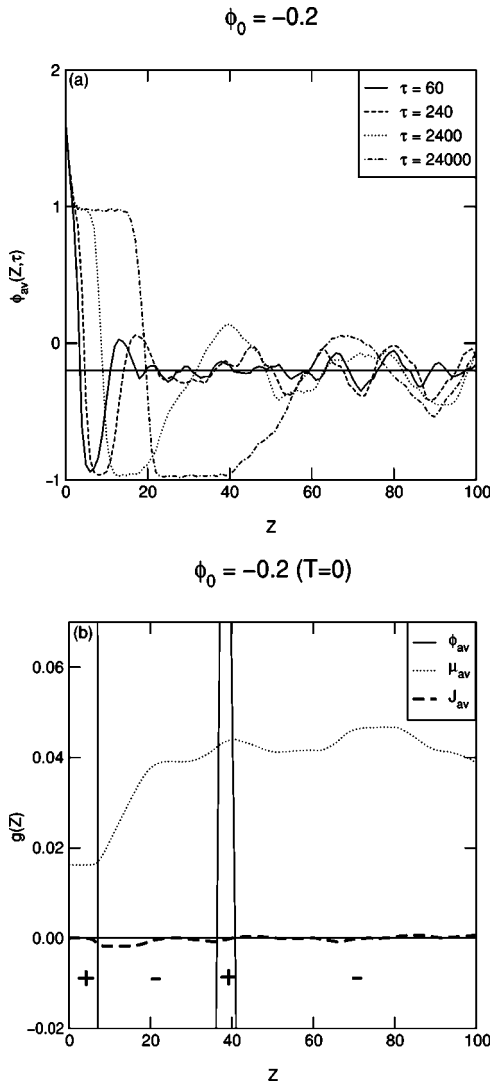

FIG. 2. (a) Plot of laterally averaged profiles, $\phi_{\rm av}(z,\tau)$ vs z, for the evolution depicted in Fig. 1. The laterally averaged profiles are obtained by averaging $\phi(x,z,\tau)$ along the x direction for a typical snapshot shown in Fig. 1. Furthermore, we average over 200 independent runs. A horizontal line is drawn at $\phi_0=-0.2$, corresponding to the average composition of the mixture. (b) Plot of laterally averaged quantities, $g(z)$ vs z, for the noiseless ($T=0$) version of the evolution depicted in Fig. 1. We present results for $g \equiv \phi_{\rm av}, \mu_{\rm av}, J_{\rm av}$ at $\tau=2400$. The chemical potential $\mu(\vec{x},\tau)$ and current $J_z(\vec{x},\tau)$ are defined in the text. The + and − signs refer to the sign of $\phi_{\rm av}(z,\tau)$ in a particular region.

and $R_2(\tau)$ denote the first and second zeros, respectively, and both of these grow with time.

It is also relevant to examine the z dependence of the chemical potential $\mu(\vec{x},\tau)$, and z current $J_z(\vec{x},\tau)=-\partial\mu/\partial z$. Figure 2(b) plots the laterally averaged quantities $\phi_{\rm av}(z,\tau)$, $\mu_{\rm av}(z,\tau)$, and $J_{\rm av}(z,\tau)$ vs z. In this case, we show data sets at $\tau=2400$ for $T=0$ [no thermal fluctuations in Eq. (1)] to obtain a better understanding of the behavior of various physical quantities. On the scale of Fig. 2(b), we only see the positive (+) and negative (−) excursions of the order-parameter profile, which are as indicated. The chemical potential is flat in the wetting layer, i.e., the current is zero and the system has equilibrated locally. The chemical potential increases through the depletion layer, giving a negative current $J_{\rm av}$ (i.e., flow of A to the wetting layer). Subsequent to the second enrichment layer, the lateral-averaging procedure does not yield a systematic behavior for $\mu_{\rm av}$ and $J_{\rm av}$.

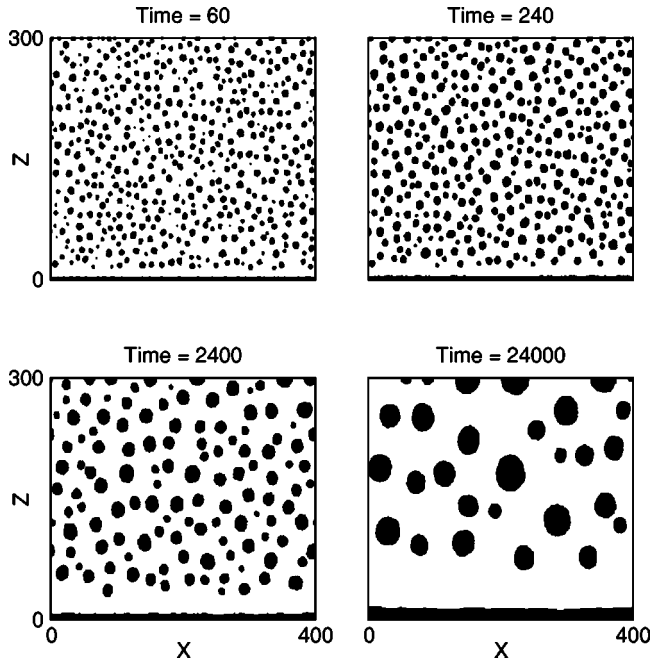

FIG. 3. Analogous to Fig. 1, but for $\phi_0=-0.6$.

Figure 3 is analogous to Fig. 1, but corresponds to the case $\phi_0=-0.6$. The mean-field spinodal is $\phi_s=1/\sqrt{3}\simeq 0.577$, so this composition lies slightly beyond the spinodal—in the ''nucleation and growth'' region of the phase diagram. Thermal noise nucleates many droplets of the minority phase in the bulk. (Note that the singular behavior at the spinodal is washed out for any nonzero noise strength [1].) These droplets coarsen, along with the wetting layer at the surface. Figure 4 shows the corresponding laterally averaged profiles. In general, the scenario is similar to that shown in Figs. 1 and 2, though the time scales of growth are slower for $\phi_0=-0.6$. (An intermediate case, $\phi_0=-0.4$, is completely analogous [26], and hence not shown here.)

Finally, we consider the evolution of an extremely off-critical case ($\phi_0=-0.8$ or 10% A and 90% B) in Fig. 5. In this case, the thermal fluctuations are not sufficient to nucleate an A-rich droplet on the time scale of our simulation. Thus, there is no phase separation in the bulk—nevertheless, there is a rapid growth of the wetting layer at the surface. Figure 6(a) shows the laterally averaged profiles corresponding to Fig. 5. Notice that the A-rich surface wetting layer is followed by a layer which is moderately depleted in A, and extends deep into the bulk. The behavior for $\phi_0=-0.8$ differs qualitatively from that for $\phi_0=-0.2,-0.6$, and we study $\mu_{\rm av}(z,\tau)$, $J_{\rm av}(z,\tau)$ vs z in Fig. 6(b). Again, we show data for the case with $T=0$ at $\tau=2400$. The chemical potential is approximately flat (and z current zero) in the wetting layer, as in Fig. 2(b). Then, $\mu_{\rm av}(z,\tau)$ increases monotonically with z (resulting in a current of A to the wetting layer), and saturates exponentially to its bulk value as $z\to\infty$.

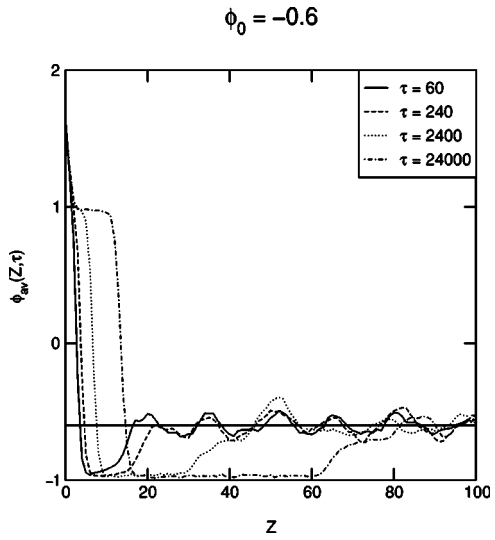

FIG. 4. Analogous to Fig. 2(a), but for $\phi_0 = -0.6$.

2. Growth kinetics of wetting layers

We are interested in understanding the time dependence of various features of the wetting profiles seen in Figs. 2(a) and 4, where the bulk undergoes phase separation. (We will focus on the case of extremely off-critical quenches later.) We denote the thickness of the depletion layer as $h(\tau) = R_2(\tau) - R_1(\tau)$.

Consider the typical evolution snapshots shown in Figs. 1 and 3. The wetting layer grows due to two contributions to the chemical-potential gradient (or current): (a) the surface-potential gradient drives A to the wetting layer with a current $dV(z)/dz|_{z=R_1}$; (b) the intrinsic chemical potential (due to local curvature) is higher on the curved surface of bulk A-rich droplets than on the flat wetting layer. This difference

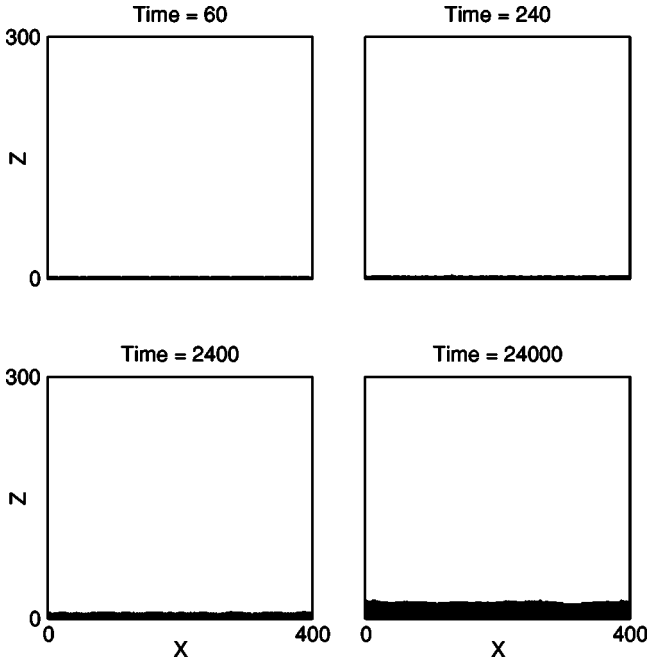

FIG. 5. Analogous to Fig. 1, but for $\phi_0 = -0.8$.

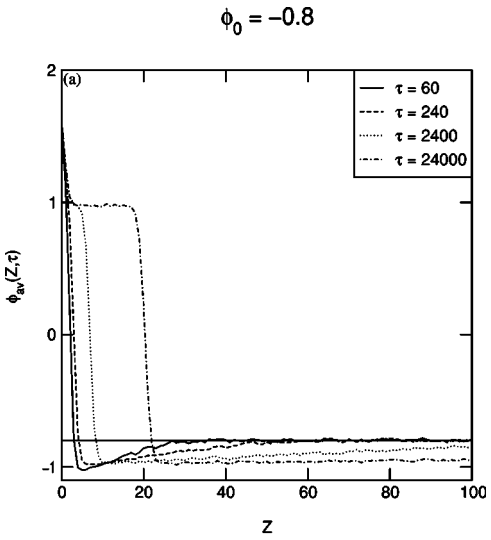

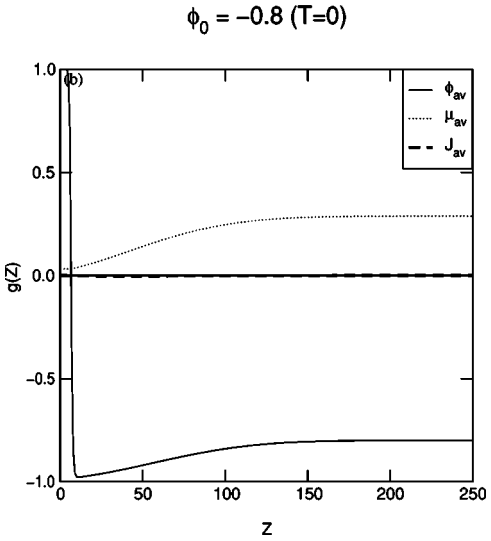

FIG. 6. Analogous to Figs. 2(a) and 2(b), but for $\phi_0 = -0.8$.

is estimated as σ/L, where $L(\tau)$ is the bulk domain size, and σ is the surface tension. (In our dimensionless units, we have $\sigma = 2/3$.) The corresponding current contribution at the wetting layer is $-\sigma/(Lh)$. Thus the A current in the z direction is

$$J_z \simeq \left.\frac{dV(z)}{dz}\right|_{z=R_1} - \frac{\sigma}{Lh}. \tag{9}$$

To estimate $h(\tau)$, we assume that the wetting and depletion layers have an overall composition of ϕ_0. This yields the relations

$$R_2(\tau) \simeq \frac{2}{1+\phi_0} R_1(\tau),$$

$$h(\tau) \simeq \frac{1-\phi_0}{1+\phi_0} R_1(\tau). \tag{10}$$

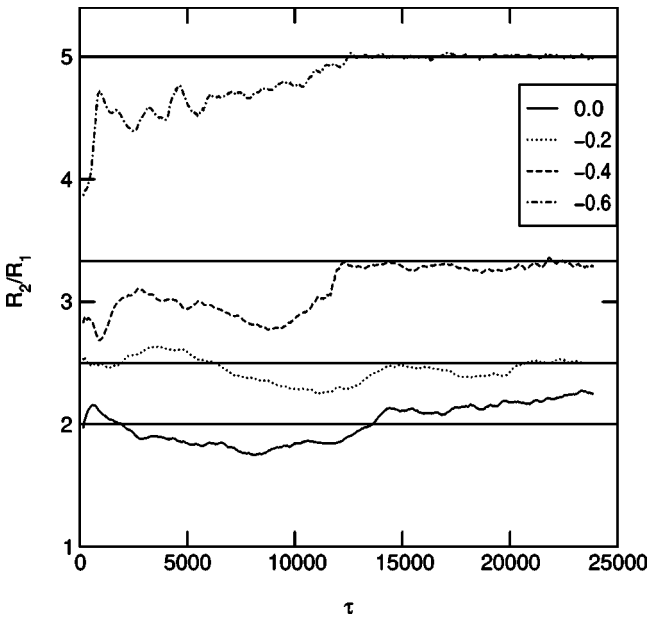

FIG. 7. Plot of R_2/R_1 vs τ for $\phi_0=0.0,-0.2,-0.4,-0.6$. We define $R_1(\tau)$ as the first z value at which $\phi_{\rm av}(z,\tau)$ crosses ϕ_0, and $R_2(\tau)$ as the second z value at which $\phi_{\rm av}(z,\tau)$ crosses ϕ_0.

Figure 7 plots R_2/R_1 vs τ for $\phi_0=0.0,-0.2,-0.4,-0.6$. The horizontal lines denote the appropriate values of $2/(1+\phi_0)$. We see that the scaling assumption of Eq. (10) is reasonable.

Using the power-law form of the potential from Eq. (2), and $h(\tau)$ from Eq. (10), Eq. (9) yields [26]

$$\frac{dR_1}{d\tau}=-J_z\simeq\frac{nh_1}{R_1^{n+1}}+\frac{\sigma}{LR_1}\left(\frac{1+\phi_0}{1-\phi_0}\right). \tag{11}$$

The bulk length scale obeys the LS growth law $L(\tau)=f(\phi_0)(\sigma\tau)^{1/3}$, where the function $f(\phi_0)$ is known analytically in the limit $|\phi_0|\to 1$ [2,3], and studied numerically for other values of ϕ_0 [33]. As R_1 grows with time, the first term on the right-hand-side (RHS) of Eq. (11) is dominant at early times (for $n>1$) and the second term is dominant at late times. This yields the growth regimes as

$$\begin{aligned} R_1(\tau)&\simeq[n(n+2)h_1]^{1/(n+2)}\tau^{1(n+2)}, \quad \tau\ll\tau_c,\\ &\simeq\sqrt{\frac{3}{f(\phi_0)}\frac{(1+\phi_0)}{(1-\phi_0)}}(\sigma\tau)^{1/3}, \quad \tau\gg\tau_c. \end{aligned} \tag{12}$$

The crossover time scale is obtained by equating the early-time and late-time length scales as (for $n>1$)

$$\tau_c\simeq[n(n+2)h_1]^{3/(n-1)}\times\left[\frac{f(\phi_0)}{3}\frac{1-\phi_0}{1+\phi_0}\right]^{3(n+2)/2(n-1)}\sigma^{-[(n+2)/(n-1)]}. \tag{13}$$

Clearly, the crossover between the potential-dependent growth regime and the universal regime ($R_1\sim\tau^{1/3}$) can be extremely delayed, depending on the various system parameters and mixture composition. This explains the observation of diverse exponents in experiments and numerical simulations. Figure 3(b) of Ref. [26] plots $\ln[R_1(\tau)]$ vs $\ln\tau$ for $\phi_0=0.0,-0.2,-0.4,-0.6$ and illustrates this crossover behavior.

Before we proceed, it is useful to discuss the applicability of the above arguments in the limit $\phi_0\to 0$. In this case, the bulk is nearly bicontinuous and has surfaces with both positive and negative curvatures. Then, it is appropriate to replace the second term on the RHS of Eq. (9) by its average value, which changes sign as ϕ_0 goes through zero. This would lead to a divergence of the crossover time in Eq. (13) as $\phi_0\to 0$. However, Figure 3(b) of Ref. [26] does not exhibit this feature because the above arguments do not account for the fact that even the $\phi_0=0$ evolution morphology is characterized by A-rich droplets in the region subsequent to the depletion layer [18,24]. These droplets are a result of the flow of A to the wetting layer through the depletion layer.

It is also relevant to separately discuss the cases of the power-law potential with $n=1$; and the short-ranged potential $V(z)=h_1\exp(-z/\delta)$, where δ is the characteristic decay length. For the case $V(z)\sim z^{-1}$, both terms on the RHS of Eq. (11) are comparable for all times, and the resultant growth law is the LS law, $R_1(\tau)\sim\tau^{1/3}$. On the other hand, the short-ranged potential yields a logarithmic early-time growth, $R_1(\tau)\sim\delta\ln(h_1\tau/\delta^2)$, which rapidly crosses over to the universal LS growth law. However, thermal fluctuations may affect the observation of the early-time logarithmic growth regime [30].

Next, let us consider the case of extremely off-critical quenches ($\phi_0\ll 0$), where there is no bulk phase separation—see Fig. 5. In this situation, there are no droplets in the bulk to feed the wetting layer. Thus, the intrinsic chemical potential in the bulk is the uniform value $\mu_0=\phi_0^3-\phi_0$. The corresponding current to the wetting layer is $-\mu_0/h$, where $h(\tau)$ is now the typical length scale on which the order parameter exponentially saturates to its bulk value—see Fig. 6(a). We neglect lateral fluctuations and assume a simple form (which is justified shortly) for $\phi(z,\tau)$ as follows:

$$\begin{aligned} \phi(z,\tau)&\simeq 1, && z<R_1(\tau),\\ &\simeq\phi_0-B_0e^{-(z-R_1)/h}, && z>R_1(\tau). \end{aligned} \tag{14}$$

The composition constraint then yields

$$h(\tau)\simeq\frac{(1-\phi_0)}{B_0}R_1(\tau). \tag{15}$$

Thus, Eq. (11) is modified as

$$\frac{dR_1}{d\tau}\simeq\frac{nh_1}{R_1^{n+1}}+\frac{\mu_0B_0}{1-\phi_0}\frac{1}{R_1}=\frac{nh_1}{R_1^{n+1}}+\frac{|\phi_0|(1+\phi_0)B_0}{R_1}. \tag{16}$$

The corresponding growth regimes in this case are (for all n)

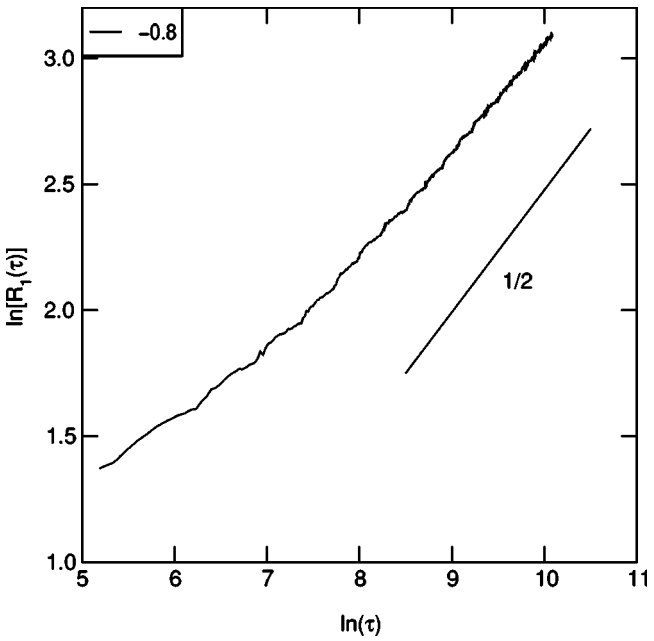

FIG. 8. Plot of $\ln[R_1(\tau)]$ vs $\ln\tau$ for $\phi_0=-0.8$. The solid line has a slope of 1/2, as indicated.

$$R_1(\tau)\simeq[n(n+2)h_1]^{1/(n+2)}\tau^{1/(n+2)}, \quad \tau\ll\tau_c,$$
$$\simeq[2|\phi_0|(1+\phi_0)B_0]^{1/2}\tau^{1/2}, \quad \tau\gg\tau_c. \quad (17)$$

Thus, there is a crossover from potential-dependent growth (as before) to a universal diffusive growth law at the crossover time

$$\tau_c\simeq[n(n+2)h_1]^{2/n}[2|\phi_0|(1+\phi_0)B_0]^{-(n+2)/n}. \quad (18)$$

Figure 8 plots $\ln[R_1(\tau)]$ vs $\ln\tau$ for $\phi_0=-0.8$ and illustrates the asymptotically diffusive growth of the wetting layer. For the short-ranged surface potential, the initial growth regime is logarithmic, as in the previous case.

We should now justify our earlier usage of the exponentially saturating profile in Eq. (14). The order-parameter profile subsequent to the wetting layer [$z>R_1(\tau)$ in Fig. 6(b)] can be approximately obtained by linearizing the deterministic ($T=0$) version of Eq. (1) about the background value ϕ_0 as $\phi(\vec{x},\tau)=\phi_0+\psi(\vec{x},\tau)$. We neglect fluctuations parallel to the surface to obtain the following linear equation for $\psi(z,\tau)$:

$$\frac{\partial\psi(z,\tau)}{\partial\tau}=(3\phi_0^2-1)\frac{\partial^2\psi(z,\tau)}{\partial z^2}-\frac{1}{2}\frac{\partial^4\psi(z,\tau)}{\partial z^4}-\frac{d^2V(z)}{dz^2}. \quad (19)$$

It is convenient to Laplace transform this equation to obtain

$$s\psi(z,s)=(3\phi_0^2-1)\frac{\partial^2\psi(z,s)}{\partial z^2}-\frac{1}{2}\frac{\partial^4\psi(z,s)}{\partial z^4}-\frac{V''(z)}{s}, \quad (20)$$

where $\psi(z,s)=\int_0^\infty d\tau e^{-s\tau}\psi(z,\tau)$, and we assume $\psi(z,0)=0$. The general solution of Eq. (20) is [34]

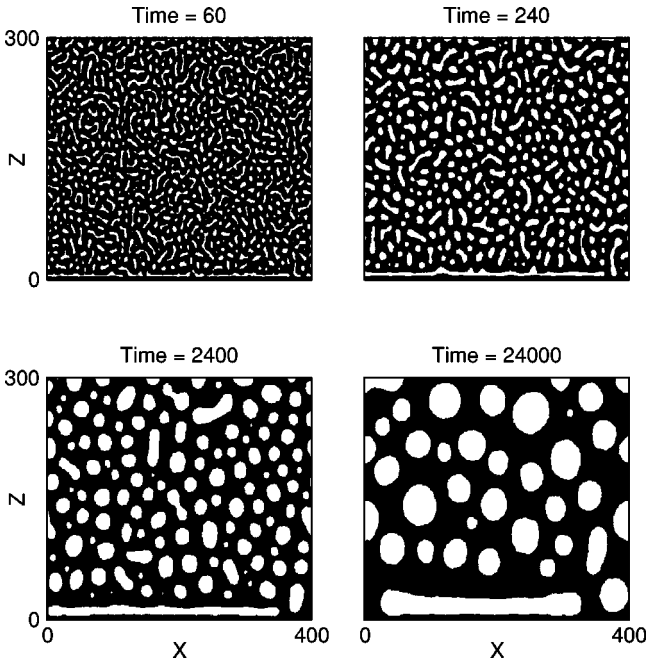

FIG. 9. Analogous to Fig. 1, but for $\phi_0=0.2$.

$$\psi(z,s)=B_+(s)e^{-z/\xi_+}+B_-(s)e^{-z/\xi_-}$$
$$+\frac{\xi_+}{s\Delta}e^{-z/\xi_+}\int_0^z dz'e^{z'/\xi_+}V''(z')$$
$$+\frac{\xi_+}{s\Delta}e^{z/\xi_+}\int_z^\infty dz'e^{-z'/\xi_+}V''(z')$$
$$-\frac{\xi_-}{s\Delta}e^{-z/\xi_-}\int_0^z dz'e^{z'/\xi_-}V''(z')$$
$$-\frac{\xi_-}{s\Delta}e^{z/\xi_-}\int_z^\infty dz'e^{-z'/\xi_-}V''(z'), \quad (21)$$

where

$$\Delta=\xi_+^{-2}-\xi_-^{-2}, \quad \xi_\pm^{-2}=(3\phi_0^2-1)\pm\sqrt{(3\phi_0^2-1)^2-2s}. \quad (22)$$

In Eq. (21), the coefficients $B_+(s)$ and $B_-(s)$ are obtained by matching the solutions for $z>R_1(\tau)$ and $z<R_1(\tau)$, which can only be done numerically in general. However, an asymptotic analysis ($s\to0$ or $\tau\to\infty$) [34] shows that ξ_+ rapidly saturates to a constant, whereas ξ_- grows diffusively ($\xi_-\sim\tau^{1/2}$) and can be identified with the "thickness" of the depletion layer $h(\tau)$.

B. Majority component wets the surface ($\phi_0>0$)

1. Evolution pictures and laterally averaged profiles

Let us next consider the case where $\phi_0>0$, so that the majority component wets the surface. Figure 9 shows the evolution of a disordered initial condition with $\phi_0=0.2$. In this case, the droplets are of the nonwetting component. A thin wetting layer is formed on the time scales of our simu-

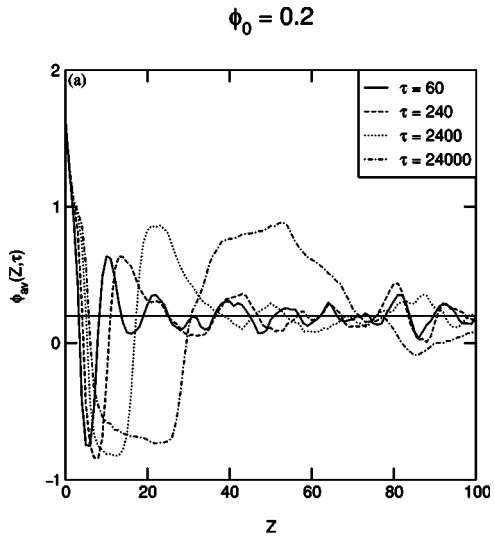

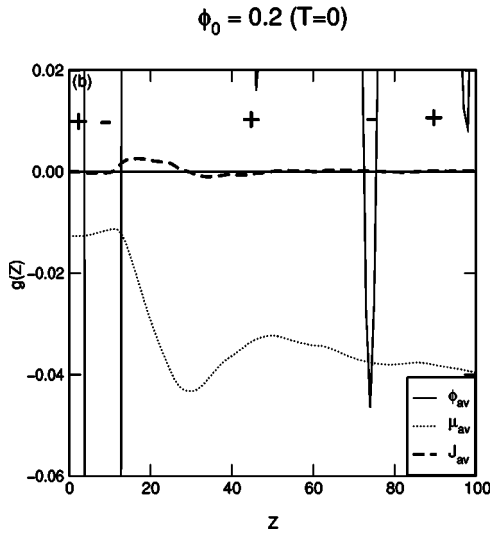

FIG. 10. Analogous to Figs. 2(a) and 2(b), but for $\phi_0 = 0.2$.

lations, and grows very slowly. The depletion layer that forms adjacent to the wetting layer consists of anisotropic droplets with a linear dimension (parallel to the wall) which diverges as $\phi_0 \to 0$. However, at $\phi_0 = 0.4$ (see Fig. 2 in Ref. [26]), the droplets forming the depletion layer are already almost spherical. Figure 10(a) shows the laterally averaged profiles corresponding to the evolution in Fig. 9, and confirms the slow growth of the wetting layer.

It is relevant to ask why the wetting layer grows so slowly in the case where the majority component wets the surface. Essentially, the bulk droplets now compete with (rather than feed) the wetting layer for the component *A*, as the intrinsic chemical potential for *A* is lower on the surface of the drops. Thus, in Eq. (9), only the first term on the RHS is operational—the intrinsic chemical-potential gradient actually drives *A* into the bulk. To clarify this, Fig. 10(b) plots $\phi_{av}, \mu_{av}, J_{av}$ vs z at $\tau = 2400$ for $T = 0$. As in Fig. 2(b), the chemical potential is flat in the wetting layer as the system has equilibrated locally. In the depletion layer, the chemical potential increases gradually—resulting in an *A* current to the wetting layer. However, the chemical potential falls

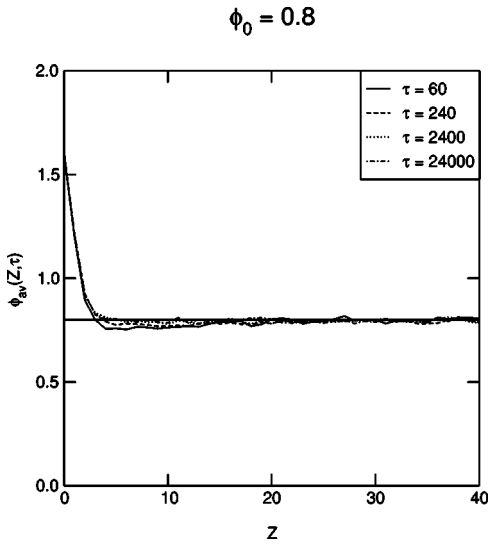

FIG. 11. Analogous to Fig. 2(a), but for $\phi_0 = 0.8$.

sharply as one moves further into the bulk—resulting in a competing *A* current to larger values of *z*. Similar considerations apply for other values of $\phi_0 > 0$, when the bulk undergoes phase separation. For the sake of brevity, we do not show evolution pictures and laterally averaged profiles for these cases here.

Finally, we consider an extremely off-critical case with $\phi_0 = 0.8$. Figure 11 shows laterally averaged profiles for this case. The corresponding evolution pictures are entirely ''black'' as there is no phase separation on the time scale of our simulation, and we do not show these here. The form of the order-parameter profiles in Fig. 11 is analogous to enrichment profiles seen for $T > T_c$, i.e., when a miscible binary mixture (AB) is placed in contact with a surface which prefers *A* [34]. The relevant dynamical equations are obtained by linearizing Eqs. (1), (5)–(6) (at $T = 0$) about ϕ_0 and neglecting lateral fluctuations. The bulk equation is already given as Eq. (19), and this should be supplemented with the linearized boundary conditions,

$$\frac{\partial \psi(0,\tau)}{\partial \tau} = V(0) + g\phi_0 + g\psi(0,\tau) + \gamma \left. \frac{\partial \psi}{\partial z} \right|_{z=0}, \qquad (23)$$

$$0 = \frac{\partial}{\partial z} \left[(3\phi_0^2 - 1)\psi - \frac{1}{2} \frac{\partial^2 \psi}{\partial z^2} - V(z) \right] \Bigg|_{z=0}. \qquad (24)$$

The general solution of Eq. (19) was already given in Eqs. (21) and (22). The complete solution to the boundary-value problem is presented in Ref. [34], and we refer the interested reader to that work. We have already discussed some asymptotic ($s \to 0$ or $\tau \to \infty$) properties of the solution—a detailed analysis is presented in Ref. [34].

2. Growth kinetics of wetting layers

It is clear from the discussion in Sec. III B 1 that the bulk droplets compete with the wetting layer for component *A*. Accretion on the wetting layer is driven by the surface-

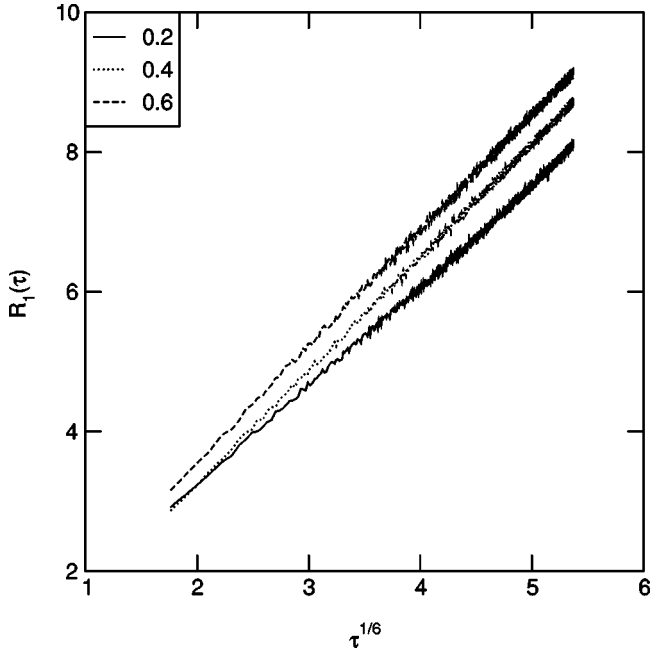

FIG. 12. Plot of $R_1(\tau)$ vs $\tau^{1/6}$ for $\phi_0=0.2,0.4,0.6$. [A log-log plot of these data sets is presented in Fig. 3(a) of Ref. [26].]

potential with the growth law $R_1(\tau)\sim\tau^{1/(n+2)}$, i.e., $R_1(\tau)\sim\tau^{1/6}$ for $n=4$ in our simulations. Figure 12 plots $R_1(\tau)$ vs $\tau^{1/6}$ for $\phi_0=0.2,0.4,0.6$. In each case, the wetting-layer kinetics is consistent with potential-driven growth. Over the time range of our simulations, we see no slowing down due to the attraction of the *A* component to the bulk droplets—we expect these effects to be manifested at later times than shown in Fig. 12.

Finally, we briefly discuss the temporal evolution of the wetting profiles in the extremely off-critical case, e.g., $\phi_0=0.8$ in Fig. 11. As discussed earlier, the evolution of profiles in this case is equivalent to the surface-enrichment problem [34] and we will directly quote results from that context. The order-parameter profiles are double exponential with one length scale $\xi_+\to$const, and the other length scale $\xi_-\to\tau^{1/2}$. The position of the first zero of the profile $[\phi(z,\tau)-\phi_0]$ grows logarithmically in time, $R_1(\tau)\sim\ln\tau$. Furthermore, all moments of the enrichment profile exhibit diffusive behavior, viz.,

$$\langle z^m\rangle=\int_0^\infty dz z^m[\phi(z,\tau)-\phi_0]\sim\tau^{m/2}. \tag{25}$$

IV. SUMMARY AND DISCUSSION

Let us conclude this paper with a summary and discussion of our results. We have undertaken a detailed analytical and numerical study of surface-directed phase separation via diffusive transport in binary mixtures with off-critical composition ($\phi_0\neq0$). The primary goal of our study is to systematize the diverse exponents observed for wetting-layer growth in various experiments and simulations.

We considered two distinct physical situations: (a) the minority component wets the surface ($\phi_0<0$); and (b) the majority component wets the surface ($\phi_0>0$). There are important differences between these two cases. For $\phi_0<0$, the wetting layer grows due to surface-potential gradients, as well as a gradient in the intrinsic chemical potential between the bulk and the wetting layer. This results in a crossover from potential-dependent growth, $R_1(\tau)\sim\tau^{1/(n+2)}$ for $V(z)\sim z^{-n}$, to universal growth. The asymptotic growth laws are $R_1(\tau)\sim\tau^{1/3}$, when the bulk undergoes phase separation; and $R_1(\tau)\sim\tau^{1/2}$, when the bulk does not phase separate.

For $\phi_0>0$, the wetting layer grows only due to surface-potential gradients. In this case, the gradient of the intrinsic chemical potential drives the preferred component into the bulk. For moderate values of ϕ_0, we find a potential-dependent growth law, $R_1(\tau)\sim\tau^{1/(n+2)}$, which is expected to slow down at later times. For $\phi_0\gg0$, the bulk does not undergo phase separation. Then, the problem of surface-directed phase separation is equivalent to the surface-enrichment problem for $T>T_c$ [34], and we have a complete analytical understanding of the evolution of order-parameter profiles. For example, the ''wetting layer'' grows logarithmically in time, $R_1(\tau)\sim\ln\tau$, and various moments of the profile exhibit diffusive behavior.

The above discussion has focused on the case of solid mixtures, where segregation occurs via diffusive transport alone. There has also been great experimental interest [35,36] in the case of fluid mixtures, where hydrodynamic modes can enable a rapid draining of the preferred component to the surface. For highly off-critical quenches, the fluid morphology is not interconnected and diffusive transport drives phase separation. In that case, the above scenario applies again. However, for smaller values of ϕ_0, the system morphology is bicontinuous and hydrodynamic effects play an important role in the kinetics of wetting and phase separation. A recent study of this has been performed by Bastea *et al.* [37], and we refer the interested reader to that work.

ACKNOWLEDGMENTS

We are grateful to H.L. Frisch for many discussions and a fruitful collaboration on related work. S.P. would like to thank H.W. Diehl, P. Fratzl, R.A.L. Jones, and H. Tanaka for useful discussions regarding these problems. One of us (S.P.) acknowledges partial support from the Deutsche Forschungsgemeinschaft under Sonderforschungsbereich 262.

[1] K. Binder, in *Materials Science and Technology, Vol. 5: Phase Transformations in Materials*, edited by R.W. Cahn, P. Haasen, and E.J. Kramer (VCH, Weinheim, 1991), p. 405.

[2] A.J. Bray, Adv. Phys. **43**, 357 (1994).

[3] A. Onuki, *Phase Transition Dynamics* (Cambridge University Press, Cambridge, 2002).

[4] I.M. Lifshitz and V.V. Slyozov, J. Phys. Chem. Solids **19**, 35 (1961).

[5] K. Binder and D. Stauffer, Phys. Rev. Lett. **33**, 1006 (1974).
[6] E.D. Siggia, Phys. Rev. A **20**, 595 (1979).
[7] H. Furukawa, Phys. Rev. A **31**, 1103 (1985).
[8] P.F. Fratzl, J.L. Lebowitz, O. Penrose, and J. Amar, Phys. Rev. B **44**, 4794 (1991).
[9] T. Young, Philos. Trans. R. Soc. London, Ser. A **95**, 69 (1805).
[10] J.W. Cahn, J. Chem. Phys. **66**, 3667 (1977).
[11] P.G. de Gennes, Rev. Mod. Phys. **57**, 827 (1985).
[12] S. Dietrich, in *Phase Transitions and Critical Phenomena: Vol. 12*, edited by C. Domb and J. L. Lebowitz (Academic, London, 1988), p. 1.
[13] R.A.L. Jones, L.J. Norton, E.J. Kramer, F.S. Bates, and P. Wiltzius, Phys. Rev. Lett. **66**, 1326 (1991).
[14] G. Krausch, J. Mlynek, W. Straub, R. Brenn, and J.F. Marko, Europhys. Lett. **28**, 323 (1994).
[15] M. Geoghegan, H. Ermer, G. Jüngst, G. Krausch, and R. Brenn, Phys. Rev. E **62**, 940 (2000).
[16] G. Krausch, Mater. Sci. Eng., R. **14**, 1 (1995).
[17] S. Puri and K. Binder, Phys. Rev. A **46**, R4487 (1992); Phys. Rev. E **49**, 5359 (1994).
[18] S. Puri, K. Binder, and H.L. Frisch, Phys. Rev. E **56**, 6991 (1997).
[19] K. Binder, S. Puri, and H.L. Frisch, Faraday Discuss. **112**, 103 (1999).
[20] G. Brown and A. Chakrabarti, Phys. Rev. A **46**, 4829 (1992).
[21] J.F. Marko, Phys. Rev. E **48**, 2861 (1993).
[22] A. Bhattacharya, M. Rao, and A. Chakrabarti, Phys. Rev. E **49**, 524 (1994).
[23] G. Brown, A. Chakrabarti, and J.F. Marko, Phys. Rev. E **50**, 1674 (1994).
[24] S. Puri and H.L. Frisch, J. Phys.: Condens. Matter **9**, 2109 (1997).
[25] K. Binder, J. Non-Equilib. Thermodyn. **23**, 1 (1998).
[26] S. Puri and K. Binder, Phys. Rev. Lett. **86**, 1797 (2001).
[27] K. Binder, Z. Phys. **267**, 313 (1974).
[28] K. Binder and H.L. Frisch, Z. Phys. B: Condens. Matter **84**, 403 (1991).
[29] I.E. Dzyaloshinskii, E.M. Lifshitz, and L.P. Pitaevskii, Adv. Phys. **10**, 165 (1961).
[30] R. Lipowsky, J. Phys. A **18**, L585 (1985).
[31] S. Puri and K. Binder, Z. Phys. B: Condens. Matter **86**, 263 (1992).
[32] S. Puri and K. Binder, J. Stat. Phys. **77**, 145 (1994); S. Puri and K. Binder (unpublished).
[33] Y. Oono and S. Puri, Phys. Rev. Lett. **58**, 836 (1987); S. Puri and Y. Oono, Phys. Rev. A **38**, 1542 (1988).
[34] S. Puri and H.L. Frisch, J. Chem. Phys. **79**, 5560 (1993); H.L. Frisch, S. Puri, and P. Nielaba, *ibid.* **110**, 10 514 (1999).
[35] P. Guenoun, D. Beysens, and M. Robert, Phys. Rev. Lett. **65**, 2406 (1990); Physica A **172**, 137 (1991).
[36] P. Wiltzius and A. Cumming, Phys. Rev. Lett. **66**, 3000 (1991); A. Cumming, P. Wiltzius, F.S. Bates, and J.H. Rosedale, Phys. Rev. A **45**, 885 (1992).
[37] S. Bastea, S. Puri, and J.L. Lebowitz, Phys. Rev. E **63**, 041513 (2001).